Proton emission following multiple electron capture in slow $N^{7+}+HCl$ collisions

F. Frémont, D. Martina, O. Kamalou, P. Sobocinski, and J.-Y. Chesnel
Centre Interdisciplinaire de Recherche Ions Lasers, Unité Mixte CEA-CNRS-EnsiCaen-Université de Caen Basse-Normandie, 6 boulevard du Mal Juin, F-14050 Caen Cedex, France

I. R. McNab
Physics, School of Natural Sciences, University of Newcastle upon Tyne, Newcastle upon Tyne NE1 7RU, United Kingdom

F. R. Bennett
CSIRO Minerals, P. O. Box 90, Bentley, Western Australia 6982, Australia
(Received 25 January 2005; published 12 April 2005)

Collisions between 98-keV N^{7+} ions and a HCl target have been investigated experimentally. The kinetic-energy distribution of fragment H^+ ions originating from multiple electron capture was detected at angles in the range 20°–160° with respect to the incident beam direction. Proton energies as large as 100 eV were observed, and calculations made in the simple Coulomb explosion model suggest that up to seven target electrons may be involved during the collision. Using the Landau-Zener model, we show that the N^{7+} projectile mainly captures outer-shell electrons from HCl. From the experimental data we derived multiple-capture cross sections which we compared with results from a model calculation made using the classical over-barrier model and also with a semiempirical scaling law. For the specific case of double capture, several structures appeared, which were assigned using *ab initio* calculations to states of HCl^{2+}.

DOI: 10.1103/PhysRevA.71.042706 PACS number(s): 34.50.Gb, 34.70.+e

I. INTRODUCTION

The study of collisions between slow highly charged ions and molecular species has received much attention during the past few years. The studies give detailed experimental [1–6] and theoretical [7–9] information both on electron capture that occurs during the collision, and on the fragmentation dynamics that take place after the removal of the electrons from the target. Much effort has been focused on understanding collisions between slow highly charged ions and simple molecular targets such as H_2 or D_2 [4–9].

Very recently, some of us performed experimental and theoretical studies of slow collisions between $O^{5+}+H_2$ and $N^{7+}+H_2$ [4,6]. We were able to analyze the influence of the projectile on the fragment energy distributions following double electron capture (DC), as a function of the projectile velocity. Three impact-velocity regions could be distinguished: (1) isotropic fragmentation at high velocities (>0.5 a.u.), (2) strong backward fragmentation at projectile velocities between 0.5 and 0.1 a.u., and (3) strong forward fragmentation at velocities less than 0.1 a.u. We now give a little more detail for each of these regimes.

(1) At relatively high projectile velocities v_P (>0.5 a.u.), the fragmentation was found to be isotropic, and the energy distributions were given, at each detection angle, by a sharp peak centered at ~9.5 eV, which corresponds to a free fragmentation [4]. At such velocities, our model calculations showed that the capture occurs mainly at large impact parameters b (5–7 a.u.), and in the "way out" of the collision, according to the notation of the over-barrier (OB) model [10]. It was concluded that, at such velocities, the influence of the projectile charge on each fragment is negligible.

(2) At impact velocities ranging from ~1 to 0.5 a.u., the fragments were found to be emitted mainly in the backward direction with respect to the incident beam direction [4,6]. This effect, also reported for the system $Xe^{26+}+D_2$ [8], is due to the strong influence of the Coulomb forces induced by the projectile which modify the fragment trajectories and energies, during and after the capture process. While the dominant capture occurs at large impact parameter ($b \approx 5$ a.u.) and on the way out of the collision, a small fraction of highly energetic fragments are also detected in the forward direction. These fragments were found to originate from electron capture at very small impact parameter ($b < 1$ a.u.), in the "way in" of the collision.

(3) At projectile velocities lower than 0.1 a.u., the fragment protons were seen to be emitted preferentially at forward angles, indicating that the capture process occurs predominantly at small impact parameters ($b < 1$ a.u.), on the "way in" to the collision. This observation is consistent with the results of previous calculations performed for the collision system $Xe^{23+}+H_2$ at a projectile energy of 1 eV/amu [9]. In addition, for this latter system as well as for the $O^{5+}+H_2$ and $N^{7+}+H_2$ systems, the double-electron-capture process was found to give the major contribution to the total cross section [4,6,9].

Slow collisions involving multielectronic molecular targets have also been studied in the last ten years [11–15]. The detailed analysis of such collisions requires data from multiple-coincidence techniques. Using these techniques, information on the fragmentation of the residual target after the capture process could be revealed. For example, in double charge exchange following very slow $Kr^{8+}+N_2$ collisions [14], many fragmentation channels involving highly charged N_2^{q+} ($q \leqslant 5$) residual target ions were identified. The role of the initial molecule orientation in the multiple ionization of

N_2 and O_2 was also studied experimentally in collisions of highly charged Xe ions at projectile velocities of ~0.2 a.u. [13].

Apart from these works, the fragmentation studies have given only minor information on the electron-capture process itself. For example, as shown previously [4,6], the impact-parameter distributions, which can be derived from the analysis of the fragmentation channels, are important to know because they give insight into the nature of the captured electrons. Moreover, the final charge-state distribution of the target may change with the projectile velocity, giving information on the number of electrons involved in the capture process. For the case of molecular targets, many questions remain to be answered, because the electronic structure of a molecule differs strongly from that of an atom and the electron capture and subsequent fragmentation of molecules depend upon the chemical bonding within each electronic state of the molecule that contributes to the observations.

In the present work we studied the fragmentation of HCl following multiple electron capture by N^{7+} projectile ions. The use of HCl was motivated by the fact that in a fragmentation process conservation of momentum leads to the H^+ fragment (of mass 1 a.u.) having a kinetic energy which is typically 35 times larger than that of the corresponding Cl^{q+} fragment (of mass 35 a.u.). Therefore, after the capture process, the dissociation of HCl leads to fragments whose energies may easily be separated. The H^+ fragments were detected as a function of their energy and for detection angles varying from 20° to 160° with respect to the incident beam direction. In the following analysis, the different reaction pathways are discussed and the charge distributions are deduced. From the fragment kinetic-energy spectra, relative cross sections for multiple electron capture are deduced, and these are compared with results derived from both the classical over-barrier model [10] and the semiempirical scaling law of Selberg *et al.* [16].

II. EXPERIMENTAL SETUP

The experimental setup has been described in detail elsewhere [17], and so only a brief description is given here. The experiments were conducted at the 14-GHz electron cyclotron resonance (ECR) ion source of the LIMBE facility, at the Grand Accélérateur National d'Ions Lourds (GANIL) in Caen. The N^{7+} ions, extracted at an energy of 98 keV, were magnetically analyzed and focused to a diameter of ~2 mm. Typical ion currents of ~50 nA were collected in a Faraday cup and these were used to normalize the spectra. In the scattering chamber, a base pressure smaller than 10^{-6} mbar was achieved. In the center of the scattering chamber, the N^{7+} beam was colliding with a gas-beam target of HCl that was created by an effusive gas jet. The average HCl target pressure was determined to be $\sim 10^{-4}$ mbar, corresponding to a residual pressure of $\sim 10^{-5}$ mbar in the chamber. These pressures were sufficiently low to ensure the predominance of single collisions. The fragments produced after the collision were detected at angles in the range from 20° to 160° with respect to the incident beam direction, using a single-stage spectrometer which consists of an electrostatic parallel-plate analyzer. The intrinsic energy resolution of the exit analyzer was 5% full width at half maximum. The fragment acceptance angle was ~2°. The length ℓ_0 of the ion beam, as seen by the spectrometer at 90°, was ~4 mm. This length, increasing according to $\ell_f = \ell_0 / \sin\theta$ as the observation angle θ decreases, was taken into account in our determination of the differential cross sections in energy and angle.

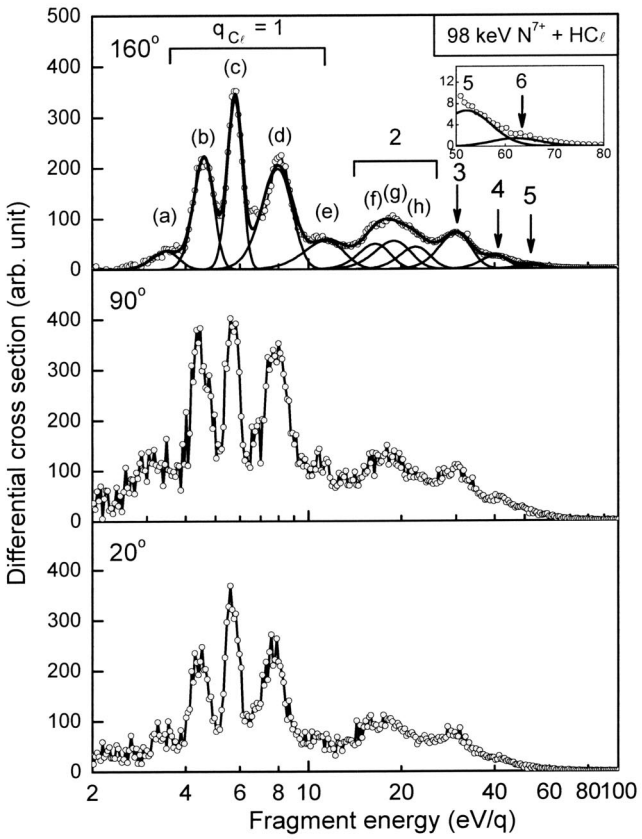

FIG. 1. Energy distribution of protons and chlorine ions (open circles) at detection angles of 20°, 90°, and 160° following the fragmentation of HCl ions after multiple capture in 98-keV N^{7+} + HCl collisions. The full curves are the results of a fit procedure of the spectrum using Gaussian curves.

III. SPECTRA ANALYSIS AND DISCUSSION

A. Role of outer- and inner-shell electrons in the capture process

Figure 1 shows fragment spectra for detection angles of 20°, 90°, and 160°. These spectra consist of several structures whose energies range from 3 to 100 eV. As explained in the Introduction, the observed peaks are attributed to protons following the Coulomb explosion of multiply charged HCl after the electron-capture process. The occurrence of high proton energies originates from multiple electron capture. In order to separate the different charge-state contributions of the target, each peak in the spectrum was fitted with Gaussian curves (only shown at 160° in Fig. 1) and the experimental energies for each peak were compared (Table I) with theoretical energies derived from the simple Coulomb explosion

TABLE I. Experimental and calculated energies of H^+ fragments following the dissociation of HCl in 98-keV N^{7+}+HCl collisions, as a function of the charge q of Cl^{q+}. The letters (a)—(h) refer to the peaks in Fig. 1.The energy E_{H^+} (column 2) is determined by fitting each peak with Gaussian curves. The uncertainties given in column 2 take into account the standard deviation in the fit procedure. The calculated mean energies are derived from the simple Coulomb explosion model (see text).

q		E_{H^+} (eV)	$\overline{E_{H^+}}$ (eV) (calc.)
1	*a*	3.0±0.1	
	b	4.5±0.1	
	c	5.8±0.1	11.3
	d	7.7±0.1	
	e	11.1±0.1	
2	*f*	15.8±0.5	
	g	19±0.5	22.6
	h	21±0.5	
3		29.1±1.0	33.9
4		40.6±1.5	45.2
5		53±4	56.5
6		63±5	67.7

model. This model assumes that the final total kinetic energy $\overline{E_{kin}}$ of the H^+ and Cl^{q+} fragments is equal to the initial Coulomb repulsion energy q/R_0, where q is the charge of the Cl^{q+} fragments (the charge of H^+ is 1), and R_0 is the internuclear distance between H and Cl at equilibrium ($R_0 \approx 2.41$ a.u.). It is first seen from Table I that H^+ fragments are associated with Cl^{q+} fragments whose charge can reach values as large as 6. This is an indication that up to seven target electrons may be active during the capture process.

For $q=1$, corresponding to energy release from HCl^{2+}, five structures are observed, suggesting that excited states of HCl^{2+} are produced in the ionization process. To our knowledge, while doubly excited states of HCl are reported in the literature, detailed information on the resulting fragment energies is missing. Only a few energies are available [18,19]. The origin of these peaks will be discussed in detail in Sec. III C.

Two reaction pathways can lead to formation of H^+ with identical kinetic energies, but we are able to use Auger spectra to discriminate between the two possibilities. The reactions that can lead to H^+ fragments are as follows.

(i) After the capture of q electrons [Eq. (1a)], the ionized molecular target may first deexcite by autoionization [Eq. (1b)] (molecular autoionization), and then dissociate [Eq. (1c)]:

$$N^{7+} + HCl \rightarrow N^{(7-q)+} + HCl q^{+*}, \tag{1a}$$

$$HCl q^{+*} \rightarrow HCl^{(q+1)+} + e^-, \tag{1b}$$

$$HCl^{(q+1)+} \rightarrow H^+ + Cl^{q+} + \overline{E_{kin}}. \tag{1c}$$

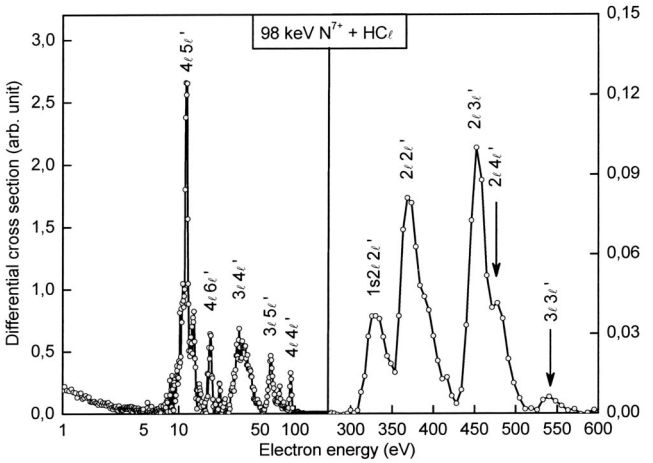

FIG. 2. Spectrum of Auger electrons produced in 98-keV N^{7+} +HCl collisions at an observation angle of 90°. The lines in the range 5–100 eV correspond to the decay of projectile states associated with $3\ell n\ell'$ and $4\ell n\ell'$ ($n \geq 4$). The lines in the range 300–600 eV are essentially due to multiple electron capture.

(ii) The projectile may also capture $(q+1)$ target electrons [Eq. (2a)], the target dissociates [Eq. (2b)]:

$$N^{7+} + HCl \rightarrow N^{(6-q)+} + HCl^{(q+1)+}, \tag{2a}$$

$$HCl^{(q+1)+} \rightarrow H^+ + Cl^{q+} + \overline{E_{kin}}. \tag{2b}$$

For both of the pathways above (i) and (ii), the Cl^{q+} ion [Eq. (1c) and (2b)] may remain in an excited state. Thus the chlorine fragments may autoionize (atomic autoionization):

$$Cl q^{+*} \rightarrow Cl^{(q+1)+} + e^-. \tag{3}$$

Both (i) and (ii) pathways lead to the same kinetic energy releases $\overline{E_{kin}}$. Therefore, in principle, a given proton energy (reported in Table I) may be associated with the capture of either q or $(q+1)$ target electrons. However, the atomic autoionization process does not depend on the fragmentation dynamics. Therefore, atomic autoionization gives rise to well-defined structures in Auger electron energy distributions [20] while in contrast, molecular autoionization produces a continuous background.

Thus, we used the Auger spectrum (measured at an observation angle of 90°) to reveal possible autoionization process of the excited target (Fig. 2). As shown in Fig. 2, two distinct groups of peaks are clearly separated. In the range 0 to 100 eV (left side of Fig. 2), double electron capture populates configurations of quasiequivalent electrons $3\ell n\ell'$ and $4\ell n\ell'$ ($n \geq 4$) of the projectile, while the lines in the range from 300 to 600 eV are essentially due to the capture of more than two electrons, which gives rise to *K* Auger electrons [21,22]. As shown by Wills *et al.* [23], the ejection of an inner-shell 4σ target electron gives rise to an Auger electron with an energy less than 3 eV. In our spectrum (Fig. 2), no peak appears at low energy (<10 eV) and the background is found to be negligible. This result indicates that the target or chlorine autoionization is unlikely to occur. Consequently, the reaction pathway (ii) is favored; the projectile captures

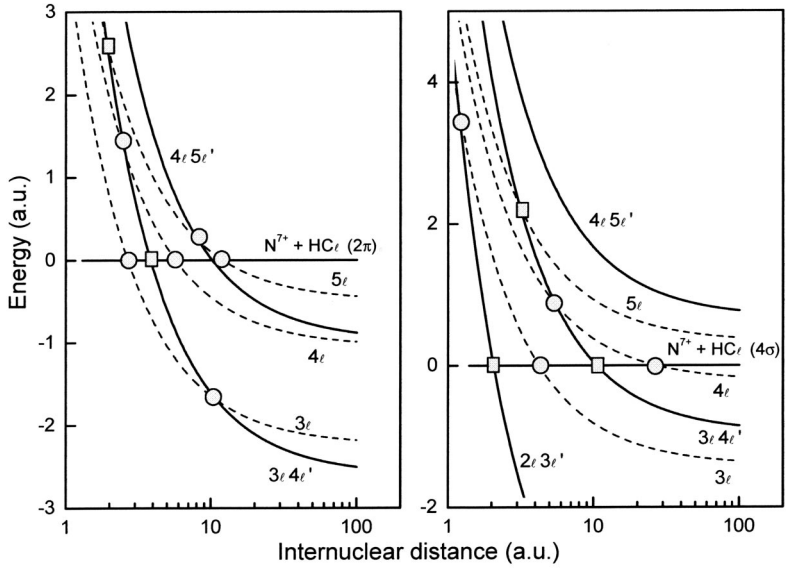

FIG. 3. Diagrams of approximate potential curves of the $N^{7+}+HCl$ system. On the left side (right side), capture of an outer-shell 2π (inner-shell 4σ) electron is supposed. Dashed lines and solid lines correspond to single and double capture, respectively.

$(q+1)$ target electrons giving rise to the $HCl^{(q+1)+}\rightarrow H^+ + Cl^{q+} + \overline{E_{\rm kin}}$ pathway.

To theoretically investigate the role of outer-shell valence electrons in the electron capture process, we applied the multichannel Landau-Zener model [24] for single (SC) and double electron capture. Very briefly, the transition probability p_{if} between initial (i) and final (f) states is given, at a curve crossing with projectile-target distance R_C, by

$$p_{if} = 1 - \exp\left(\frac{-2\pi|H_{if}|^2}{v_r(b)\Delta F(R_C)}\right). \tag{4}$$

In this expression, b is the impact parameter, $v_r(b)$ is the radial velocity, and $\Delta F(R_C)$ is a measure of the relative inclination of the potential curves at crossing R_C. For SC and DC, $\Delta F(R_C)=(q-1)/R_c^2$ and $\Delta F(R_C)=(q-3)/R_c^2$, respectively. The matrix element H_{if}, which describes the interaction at R_C, was calculated by using the formula derived by Olson and Salop [25].

To evaluate the crossing radii R_C, diagrams for approximate potential curves of the $N^{7+}+HCl$ system were used (Fig. 3). It is recalled that the electronic ground state of HCl is $(1\sigma^2 2\sigma^2 3\sigma^2 1\pi^4 4\sigma^2 5\sigma^2 2\pi^4)^1\Sigma^+$. The capture of outer-shell 2π (or 5σ) and inner-shell 4σ electrons is described on the left and right sides of Fig. 3, respectively. The entrance channel $N^{7+}+HCl(2\pi)$ crosses the $N^{6+}(n\ell)+HCl^+$ (with $n=3$, 4, and 5) channels (circles) at internuclear distances of $\sim$2.7, 5.7, and 12 a.u., respectively, where resonance conditions for a single transition are created for the first transition. At $\sim$2.6 and 8.2 a.u., further crossings (circles) allow a second transition from $N^{6+}(4\ell)+HCl^+$ to $N^{5+}(3\ell 4\ell')+HCl^{2+}$ and from $N^{6+}(5\ell)+HCl^+$ to $N^{5+}(4\ell 5\ell')+HCl^{2+}$. It is recalled that both $3\ell 4\ell'$ and $4\ell 5\ell'$ configurations are dominantly populated, as shown in the Auger spectrum of Fig. 2. Figure 3 also shows that the $3\ell 4\ell'$ and $4\ell 5\ell'$ configurations can also be created via dielectronic transitions (squares in Fig. 3), at internuclear distances of $\sim$2 and 3.8 a.u., respectively. The determination of the dielectronic matrix element H_{if} which describes the dielectronic transitions is by no means straightforward. Nevertheless, according to previous evaluations [26], a reasonable value of 0.05 a.u. for H_{if} was retained in our calculations.

The situation is quite different in the case of a capture of an inner-shell 4σ electron (right side of Fig. 3). First, no crossing appears between the entrance channel and the final channels $N^{6+}(5\ell)+HCl^+$ and $N^{5+}(4\ell 5\ell')+HCl^{2+}$. Consequently, the capture of 4σ electrons into 5ℓ and $4\ell 5\ell'$ configurations is unlikely to occur. The capture of 4σ electrons into 4ℓ and $3\ell 4\ell'$ configurations are also expected to give rise to negligible cross sections, because the transitions occur at large internuclear distances (>20 a.u. for 4ℓ). Consequently, the major contribution would be due to a capture into 3ℓ and $2\ell 3\ell'$ configurations, since the corresponding transitions occur at projectile-target distances ranging from $\sim$2 to 4 a.u.

In Fig. 4, the calculated differential cross sections $d\sigma/db=2\pi bP(b)db$, where $P(b)=p_{if}(1-p_{if})$ is the capture probability, are shown as a function of the impact parameter b, in the case of capture of a 2π electron (left side) and a 4σ electron (right side). The capture of one outer-shell electron gives rise mainly to a 5ℓ orbital of the projectile, while the 3ℓ orbital is mainly populated when an inner-shell electron is involved. As mentioned above, the configurations $3\ell 4\ell'$ and $4\ell 5\ell'$ $(2\ell 3\ell')$ are dominantly populated when two outer-shell (inner-shell) electrons are active during the double capture process.

The cross sections $\sigma^{2\pi}$ and $\sigma^{4\sigma}$ for the capture of outer- and inner-shell electrons, respectively, were determined by integration of $d\sigma/db$ over the impact parameter b (Table II). In addition, the ratio $\sigma^{4\sigma}/(\sigma^{2\pi}+\sigma^{4\sigma})$ is reported. For a single electron capture, the role of a 4σ electron is not negligible, since the corresponding cross section represents $\sim$23% of the total single-capture cross section. Nevertheless, this ratio decreases to $\sim$9% for a double electron capture. This finding is consistent with our experiment where no target autoionization is found (Fig. 2). Hence, it is reasonable to neglect in the following the role of 4σ electrons in the multiple electron capture process.

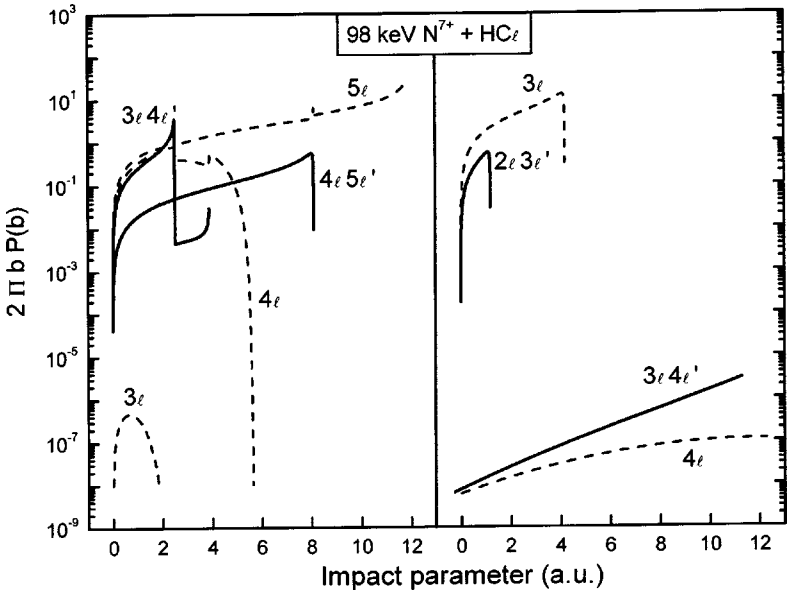

FIG. 4. Differential cross sections $d\sigma/db = 2\pi bP(b)db$ as a function of the impact parameter b, for 98-keV N^{7+}+HCl collisions, in the case of capture of 2π (left side) and 4σ (right side) electrons.

B. Energy position of the fragments

When varying the observation angle θ_d, a detailed analysis of the spectra reveals a small shift ($\ll 0.5$ eV) for fragments that follow a DC process. This result contrasts with that found for the $O^{5+}+H_2$ system at a projectile energy of 105 keV [27]. For this system, it was found that the mean energy of H^+ following the fragmentation of H_2^{2+} increases when increasing θ_d (from ~8.9 eV at 20° up to 10 eV at 160°). The shift of ~1 eV was interpreted using a two-step model, based on two successive two-body interactions [4]. In the first step, after the capture process, the residual target recoils with a velocity $\vec{v}_r$. Then, in the second step, the ion dissociates with a velocity $\vec{v}_f^{\,\text{c.m.}}$ in the frame of the molecular center of mass. Thus, the detected proton, whose velocity is defined by $\vec{v}_f^{\,L}=\vec{v}_f^{\,\text{c.m.}}+\vec{v}_r$, can have energy in the range $(E_{\min},E_{\max})$ with

$$E_{\min}=\frac{1}{2}m_{\text{H}}(v_f-v_r)^2, \tag{5a}$$

TABLE II. Cross sections $\sigma^{2\pi}$ and $\sigma^{4\sigma}$ for the single and double capture of outer- and inner-shell electrons, respectively, in 98-keV N^{7+}+HCl collisions, calculated by means of the multichannel Landau-Zener model [24]. In the last column, the ratio $\sigma^{4\sigma}/(\sigma^{2\pi}+\sigma^{4\sigma})$ is given.

Configurations	$\sigma^{4\pi}$ (cm^2)	$\sigma^{4\sigma}$ (cm^2)	$\sigma^{4\sigma}/(\sigma^{2\pi}+\sigma^{4\sigma})$
3ℓ	1.3×10^{-23}	3.9×10^{-16}	
4ℓ	6.1×10^{-17}	2×10^{-23}	
5ℓ	1.2×10^{-15}		
Total	1.26×10^{-15}	3.9×10^{-16}	0.23
$2\ell3\ell'$		6.7×10^{-18}	
$3\ell4\ell'$	3.6×10^{-17}	1.7×10^{-22}	
$4\ell5\ell'$	3×10^{-17}		
Total	6.6×10^{-17}	6.7×10^{-18}	0.09

$$E_{\max}=\frac{1}{2}m_{\text{H}}(v_f+v_r)^2, \tag{5b}$$

where m_{H} is the proton mass.

To determine $E_{\min}$ and $E_{\max}$ for N^{7+}+HCl collisions, it is necessary to estimate the residual target recoil velocity v_r.

The mean energy of the recoiling residual target is evaluated using the momentum and energy conservation laws, which result in the following expressions for the longitudinal $p_\parallel$ and transverse $p_\perp$ momenta of the recoiling target given in the laboratory frame,

$$p_\parallel \approx -\frac{Q}{v_{\text{proj}}}-\frac{n_c v_{\text{proj}}}{2}, \tag{6a}$$

$$p_\perp \approx \theta P_0. \tag{6b}$$

In these expressions Q is the inelastic energy transfer, n_c is the number of captured electrons, θ is the scattering angle of the projectile, and P_0 is the initial projectile momentum.

To simplify, we only treat the case of a DC process. The angle θ is then given by

$$\theta \approx \frac{1}{2\,E_p R_{\text{DC}}}\left[2(q_p-2)+(q_p-1)\sqrt{1-\left(\frac{R_{\text{DC}}}{R_{\text{SC}}}\right)^2}\right], \tag{7}$$

where E_p and q_p are the projectile energy and charge, respectively, and R_{SC} and R_{DC} refer to the projectile-target distances at which a SC and a DC occur. Then the average momentum $p_r=(p_\parallel^2+p_\perp^2)^{1/2}$ of the recoiling target and the corresponding recoil velocity v_r were deduced (Table III).

The results for $E_{\min}$ and $E_{\max}$ are given, assuming capture into the $3\ell4\ell'$ and $4\ell5\ell'$ configurations and a typical mean H^+ energy of 5 eV (Table III). For comparison, the results for the collision system $O^{5+}+H_2$ [4] are also reported. It is seen that, due to the difference between the target masses, the recoil velocity of the HCl target is significantly smaller than that of the H_2 target. In addition, the fragment velocity v_f is much larger than the recoil velocity v_r for N^{7+}+HCl colli-

TABLE III. Energies E_{min} and E_{max} that can reach a proton after the dissociation of HCl following a DC process. The scattering angle θ is determined from relation (7). The longitudinal and transverse components of the recoil-ion momentum are then deduced from relations (6a) and (6b). The quantities Q, R_{SC}, and R_{DC} are evaluated from the potential-energy curves of Fig. 3. For comparison, the results for the collision system $O^{5+}+H_2$ [4] are also reported.

N^{7+}+HCl	R_{SC} (a.u)	R_{DC} (a.u)	Q (a.u)	θ (rad)	$p_\perp$ (a.u)	$p_\parallel$ (a.u)	p_r (a.u)	v_r (a.u)	v_f (a.u)	E_{min} (eV)	E_{max} (eV)
$N^{5+}(4\ell 5\ell')$	11.8	8.3	0.98	3.4×10^{-4}	4.7	−2.4	5.3	7.8×10^{-5}	0.014	4.945	5.055
$N^{5+}(3\ell 4\ell')$	5.7	2.5	2.61	1.2×10^{-3}	16.9	−5.6	17.8	2.6×10^{-4}	0.014	4.82	5.19
$O^{5+}+H_2$	4.9	6.1	1.03	1.2×10^{-3}	1.6	−2.1	2.6	7.2×10^{-4}	0.0195	8.8	10.2

sions (Table III). Thus, while a shift of ~1.1 eV is observed in H^+ energy distributions for $O^{5+}+H_2$ collisions, the difference between E_{min} and E_{max} is found to be smaller than 0.4 eV in the present work. This result is in agreement with the shift observed in the experiment.

C. Experimental kinetic-energy releases and comparisons to results from model calculations

It is not the purpose of the present work to perform an exhaustive analysis of the kinetic-energy spectra. Rather, in order to show what is involved in a full calculation, we now consider in detail the kinetic-energy releases that arise from the Coulomb explosion of HCl^{2+} (peaks *a*–*e* of Fig. 1) and reserve for future work the calculations relating to the more highly charged molecular species. To assign the measured kinetic-energy releases we calculated potential-energy curves for the ground state of HCl, and for the electronic states of HCl^{2+} shown in Table IV. The states correspond to those shown in Fig. 1 of Ref. [28]. We included states with Cl^{2+} +H dissociation channels because we did not wish to assume that the fragmentation process was adiabatic. All possible nonadiabatic energy release channels were considered in our assignment.

The potential-energy curves were calculated using the MOLPRO program package [29] using similar methodology to that of Ref. [30]. Multireference configuration-interaction wave functions [31,32] based on state-averaged multiconfiguration self-consistent-field (MCSCF) [33,34] molecular orbitals were calculated for each electronic state considered. The basis set used was Dunning's cc-pV5Z generally contracted Gaussian basis [35], which in previous work [36] gave excellent agreement with vibrationally resolved experimental data for the $X\,^3\Sigma^-$ and $a\,^1\Delta$ states.

To calculate the dissociation asymptotes we calculated one potential-energy point at $d=50$ Å for each potential. By 50 Å the potentials are purely Coulombic and dissociation asymptotes for each potential were therefore calculated as

$$V(\infty) = V(d) - \frac{e^2}{4\pi\varepsilon_0}\frac{1}{d} = V(d) - 0.29 \text{ eV}.$$

We assigned the kinetic-energy release spectra as follows. We assumed that the ionization process was Franck-Condon in nature and calculated Franck-Condon factors for excitations from the ground state of HCl into the bound states and continua of HCl^{2+} using Le Roy's programs LEVEL [37] and BCONT [38], as described in [36]. In this work final energies for each state were calculated relative to the dissociation asymptote of the state itself (adiabatic fragmentation), or a lower-lying state (nonadiabatic fragmentation). The resulting theoretical energy spectra were each independently convoluted with an instrument function and then fitted with a Gaussian to find the energy releases reported in Table V. We found that states corresponding to the uppermost three dissociation limits do not contribute to the observed structure.

Our final assignments are given in Table V. Calculations and experiment are in agreement between 0.1 and 0.5 eV, except for one nonadiabatic channel. Two cases of nonadiabatic dissociation are found, and correspond to spin-orbit-mediated coupling between the $a\,^1\Delta$ and the $1\,^3\Pi$, and between the $b\,^1\Sigma^+$ and $1\,^3\Pi$ states. These couplings are strong

TABLE IV. Calculated electronic states and asymptotic energies $V(\infty)$ after the dissociation of the HCl^{2+} molecular ion.

Dissociation limit	Electronic states	$V(\infty)$ (eV)
$Cl^+(^3P_g)+H^+$	$X\,^3\Sigma^-, 1\,^3\Pi$	−459.2215
$Cl^+(^1D_g)+H^+$	$a\,^1\Delta, b\,^1\Sigma^+, 1\,^1\Pi$	−459.1691
$Cl^+(^1S_g)+H^+$	$2\,^1\Sigma^+$	−459.0956
$Cl^{2+}(^4S_u)+H$	$c\,^5\Sigma^-, 2\,^3\Sigma^-$	−458.8643
$Cl^{2+}(^2D_g)+H$	$2\,^3\Pi, 2\,^1\Pi, 1\,^1\Sigma^-, 2\,^1\Delta, 3\,^3\Sigma^-, 1\,^3\Delta$	−458.7801

TABLE V. Measured E_{expt} and calculated E_{calc} kinetic-energy releases (in eV) and assignments. In the third column, the difference ΔE between E_{calc} and E_{expt} is given. The assignments given in parentheses are the only possible nonadiabatic energy releases (see text).

Peak	E_{expt} (eV)	E_{calc} (eV)	ΔE (eV)	Assignment	
				Excitation	Dissociation
a	3.5				
b	4.6	4.63	0.03	$X\,^3\Sigma^-$	$X\,^3\Sigma^-$
b	4.6	4.71	0.11	$a\,^1\Delta$	$a\,^1\Delta$ (weak)
c	5.8	5.92	0.12	$b\,^1\Sigma^+$	$b\,^1\Sigma^+$ (weak)
c	5.8	(6.14	0.34	$a\,^1\Delta$	$1\,^3\Pi$) (strong)
c	5.8	(7.35	1.55	$b\,^1\Sigma^+$	$1\,^3\Pi$) (strong)
d	8.0	(7.35	−0.65	$b\,^1\Sigma^+$	$1\,^3\Pi$) (strong)
d	8.0	8.47	0.47	$1\,^1\Pi$	$1\,^1\Pi$
d	8.0	8.51	0.51	$1\,^3\Pi$	$1\,^3\Pi$
e	11.4	11.49	0.09	$2\,^1\Sigma^+$	$2\,^1\Sigma^+$

TABLE VI. Relative single-differential cross sections $d\sigma_{q_t}/d\Omega$ (in arbitrary units) for fragment emission associated with a given charge q_t of the residual molecular target, as a function of the observation angle θ_d.

	$d\sigma_q/d\Omega$					
θ_d	2	3	4	5	6	7
20°	1123±62	598±53	873±85	157±87	120±51	20±10
30°	991±27	723±156	502±69	292±140	102±50	27±12
40°	852±33	591±28	599±90	154±90	102±55	20±10
50°	873±49	496±28	539±42	204±48	80±40	30±15
60°	814±116	529±36	485±90	248±50	61±30	19±10
70°	786±47	643±28	414±43	214±49	114±48	36±20
80°	948±47	549±37	526±53	242±142	84±40	34±15
90°	1275±75	757±40	781±70	400±70	137±60	30±15
160°	1175±54	790±55	621±49	346±62	114±60	8±5

because of curve crossings. The majority of the intensity in the peaks comes from quasibound levels trapped behind the barriers [39]. The quasibound levels predissociate predominantly by spin-orbit interaction (a nonadiabatic process), with lifetimes calculated to be at least two orders of magnitude shorter than adiabatic predissociation by tunneling [30]. Therefore, in both cases dissociation through the nonadiabatic channel should be far stronger than adiabatic dissociation.

The worst agreement between experiment and theory is for the nonadiabatic channel $b\ ^1\Sigma^+ \rightarrow 1\ ^3\Pi$, and it is not clear whether this channel should be assigned to peak *c* or *d* (both assignments are given in Table V). The energy of the adiabatic dissociation channel $b\ ^1\Sigma^+ \rightarrow b\ ^1\Sigma^+$ *does* agree well with the measured energy of peak *c*, but unless the lifetime calculations of Ref. [30] were in error by two orders of magnitude, this must be a minor dissociation channel. In previous work by others [18], the nonadiabatic channels do not appear to have been considered, but the propensity to follow the nonadiabatic dissociation channel for both the $a\ ^1\Delta$ and $b\ ^1\Sigma^+$ states is high.

D. Experimental cross sections and comparison with model calculation

The measured fragment emission spectra were used to evaluate single-differential cross section $d\sigma_{q_t}/d\Omega$ for H^+ emission associated with a given charge q_t ($q_t=q+1$) of the residual target. Thus, the corresponding fragment energy distributions (Fig. 1) were integrated with respect to the fragment energy. The results are given in Table VI and Fig. 5. The relative statistical uncertainties are of the order of 15% for small q_t and increase to ~50% for $q_t=7$. Cross sections are found to be isotropic, within the error bars. From this result, we can conclude that the influence of the projectile Coulomb field on the H^+ fragments is negligible for the investigated impact energy.

The cross sections σ_{q_t} for the capture of q_t target electrons were determined by integration of $d\sigma_{q_t}/d\Omega$ over the observation angle. Our experimental cross sections were compared (Fig. 6) with model calculations derived from the over-barrier model [10] and from the semiempirical scaling law by Selberg *et al.* [16], which is devoted to multiple capture in slow ion-atom collisions. The experimental double-capture cross section was normalized to that obtained with the OB model. The results are presented in Fig. 6.

Neither the OB model nor the scaling law is satisfactory to fully reproduce the experimental cross sections. The dis-

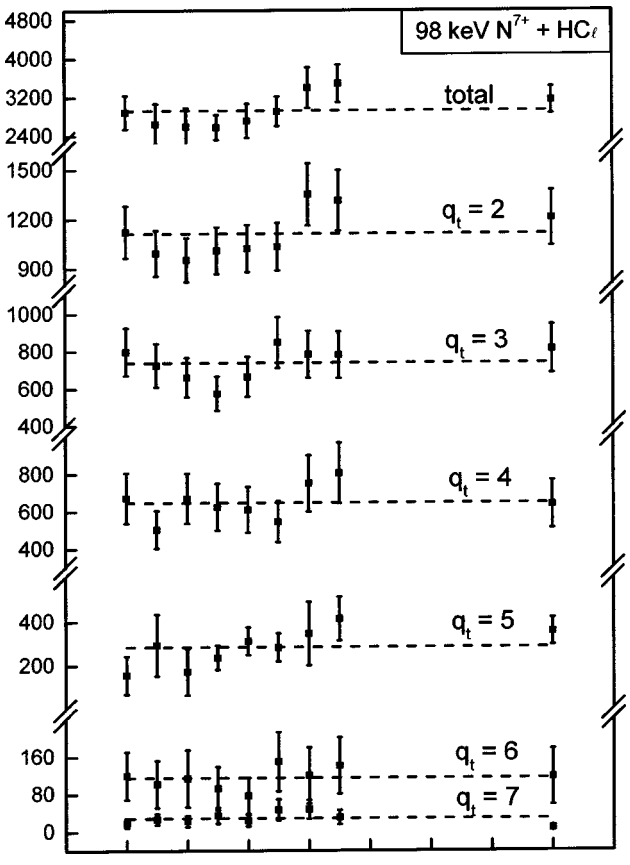

FIG. 5. Relative single-differential cross sections $d\sigma_{q_t}/d\Omega$ (in arbitrary units) for fragment emission associated with a given charge q_t of the residual molecular target, as a function of the observation angle θ_d. The averaged cross sections (dashed horizontal lines) are used as a guide for the eyes.

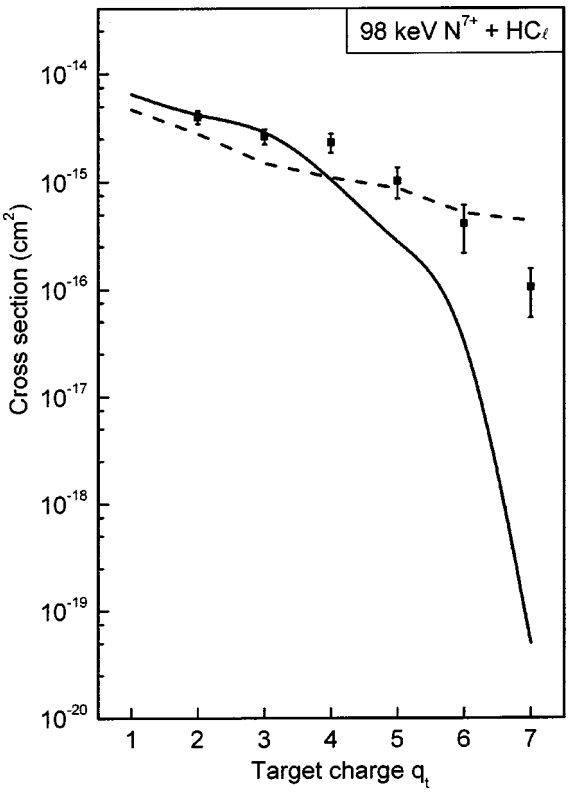

FIG. 6. Cross sections σ_{q_t} for the capture of q_t target electrons determined by integration of $d\sigma_{q_t}/d\Omega$ over the observation angle, in 98-keV N^{7+}+HCl collisions. The full squares are the results of experiment. The dashed curve is derived from the semiempirical scaling law by Selberg *et al.* [16], and the full curve is the result of the over-barrier model [10].

agreement is much more pronounced for the OB model, which gives negligible cross sections for the capture of seven electrons. In contrast, the scaling law shows a similar behavior to the experiment, since the cross sections do not differ by more than a factor of 2, except for the capture of seven electrons. This qualitative agreement indicates that, at such projectile energies, the HCl target can be viewed by the projectile as an atom.

IV. CONCLUSION

The collision system 98-keV N^{7+}+HCl has been studied by means of ion and electron spectroscopy. Fragments with energy as high as 100 eV are observed. We first showed using the Landau-Zener model [24] that the projectile mainly captures outer-shell electrons. Consequently, the Auger deexcitation of the target is negligible. Thus, our spectra indicate that the proton energy is directly connected to the number of captured electrons (up to seven).

In contrast with previous studies involving H_2 targets [4,6,12,27], the energy shift due to the recoil of the residual ionized target is found to be negligible. This is due to the fact that the HCl mass is much larger than that for H_2. Moreover, for the DC contribution, several peaks are observed, indicating that excited states of the HCl^{2+} molecular ion are populated during the collision. The kinetic energy of the H^+ fragments following the production of these excited states could be calculated. Calculations and experiment are found to be in good agreement.

Finally, the experimental cross sections were determined, as a function of the target charge, and compared with the over-barrier model [10] and a semiempirical scaling law for collisions between highly charged ions and multielectronic targets [16]. While large discrepancies are observed for the OB model, a reasonable agreement is seen for the scaling law.

This study shows that the detection of fragments is an efficient tool to obtain information on the primary process (i.e., capture). In the future, we plan a more systematic study of the electron capture process in N^{7+}+HCl collisions at lower projectile energies (down to a few eV). The goal of this work would be first to see the influence of the projectile velocity on the charged fragments, in order to obtain the impact-parameter distributions, since the capture process strongly depends on the impact parameter. Second, the dependence of the number of captured electrons, as well as their nature (outer shell, inner shell, and core electrons), on the projectile velocity will be analyzed.

[1] H. O. Folkerts, R. Hoekstra, and R. Morgenstern, Phys. Rev. Lett. **77**, 3339 (1996).
[2] B. R. Beck, J. Steiger, G. Weinberg, D. A. Church, J. McDonald, and D. Schneider, Phys. Rev. Lett. **77**, 1735 (1996).
[3] M. Tarisien, L. Adoui, F. Frémont, and A. Cassimi, Phys. Scr., T **80**, 182 (1999).
[4] P. Sobocinski, J. Rangama, J-Y. Chesnel, M. Tarisien, L. Adoui, A. Cassimi, X. Husson, and F. Frémont, in *Application of Accelerators in Research and Industry*, edited by J. L. Duggan and I. L. Morgan, AIP Conf. Proc. No. 576 (AIP, Melville, NY, 2001), p. 114.
[5] D. M. Kearns, R. W. McCullough, and H. B. Gilbody, J. Phys. B **35**, 4335 (2002).
[6] P. Sobocinski, J. Rangama, G. Laurent, L. Adoui, A. Cassimi, J-Y. Chesnel, A. Dubois, D. Hennecart, X. Husson, and F. Frémont, J. Phys. B **35**, 1353 (2002).
[7] C. J. Wood and R. E. Olson, Phys. Rev. A **59**, 1317 (1999).
[8] C. R. Feeler, R. E. Olson, R. D. DuBois, T. Schlathölter, O. Hadjar, R. Hoekstra, and R. Morgenstern, Phys. Rev. A **60**, 2112 (1999).
[9] R. E. Olson and C. R. Feeler, J. Phys. B **34**, 1163 (2001).
[10] A. Niehaus, J. Phys. B **19**, 2925 (1986).
[11] M. Tarisien, L. Adoui, F. Frémont, D. Lelièvre, L. Guillaume, J-Y. Chesnel, H. Zhang, A. Dubois, D. Mathur, S. Kumar, M. Krishnamurthy, and A. Cassimi, J. Phys. B **33**, L11 (2000).
[12] P. Sobocinski, J. Rangama, J-Y. Chesnel, M. Tarisien, L. Adoui, A. Cassimi, X. Husson, and F. Frémont, J. Phys. B **34**, L367 (2001).

[13] B. Siegmann, U. Werner, R. Mann, Z. Kaliman, N. M. Kabachnik, and H. O. Lutz, Phys. Rev. A **65**, 010704(R) (2001).
[14] T. Kaneyasu, T. Azuma, M. Ehrich, M. Yashino, and K. Okuno, Nucl. Instrum. Methods Phys. Res. B **205**, 624 (2003).
[15] Z. D. Pesic, J-Y. Chesnel, R. Hellhamer, B. Sulik, and N. Stolterfoht, J. Phys. B **37**, 1405 (2004).
[16] N. Selberg, C. Biedermann, and H. Cederquist, Phys. Rev. A **54**, 4127 (1996).
[17] F. Frémont, K. Sommer, D. Lecler, S. Hicham, P. Boduch, X. Husson, and N. Stolterfoht, Phys. Rev. A **46**, 222 (1992).
[18] S. Harper, P. Calandra, and S. D. Price, Phys. Chem. Chem. Phys. **3**, 741 (2001).
[19] R. Abusen, F. R. Bennett, I. R. McNab, D. N. Sharp, R. C. Shiell, and C. A. Woodward, J. Chem. Phys. **108**, 1761 (1998).
[20] P. Sobocinski, J. Rangama, J-Y. Chesnel, M. Tarisien, L. Adoui, A. Cassimi, X. Husson, and F. Frémont, J. Phys. B **34**, L367 (2001).
[21] P. Benoit-Catin, A. Bordenave-Montesquieu, M. Boudjema, A. Gleizes, S. Dousson, and D. Hitz, J. Phys. B **21**, 3387 (1988).
[22] F. Frémont, C. Bedouet, J-Y. Chesnel, H. Merabet, X. Husson, M. Grether, A. Spieler, and N. Stolterfoht, Phys. Rev. A **54**, R4609 (1996).
[23] A. A. Wills, D. Cubric, M. Ukai, F. Currell, B. J. Goodwin, T. Reddish, and J. Comer, J. Phys. B **26**, 2601 (1993).
[24] L. D. Landau, Phys. Z. Sowjetunion **2**, 46 (1932); C. Zener, Proc. R. Soc. London, Ser. A **137**, 696 (1932).
[25] R. E. Olson and A. Salop, Phys. Rev. A **14**, 579 (1976).
[26] C. Bedouet, F. Frémont, J-Y. Chesnel, X. Husson, H. Merabet, N. Vaeck, N. Zitane, B. Sulik, M. Grether, A. Spieler, and N. Stolterfoht, Phys. Rev. A **59**, 4399 (1999).
[27] F. Frémont, C. Bedouet, M. Tarisien, L. Adoui, A. Cassimi, A. Dubois, J-Y. Chesnel, and N. Stolterfoht, J. Phys. B **33**, L249 (2000).
[28] A. Banichevich, S. D. Peyerimhoff, M. C. Van Hemert, and P. G. Fournier, Chem. Phys. **121**, 351 (1988).
[29] H-J. Werner and P. J. Knowles with contributions from J. Almlöf, R. D. Amos, S. T. Elbert, W. Meyer, E-A. Reinsch, R. M. Pitzer, A. J. Stone, and P. R. Taylor, Computer code MOLPRO.
[30] F. R. Bennett and I. R. McNab, Chem. Phys. Lett. **251**, 405 (1996).
[31] P. J. Knowles and H-J. Werner, Chem. Phys. Lett. **145**, 514 (1988).
[32] H-J. Werner and P. J. Knowles, J. Chem. Phys. **89**, 5803 (1988).
[33] P. J. Knowles and H-J. Werner, Chem. Phys. Lett. **115**, 259 (1985).
[34] H-J. Werner and P. J. Knowles, J. Chem. Phys. **82**, 5053 (1985).
[35] T. H. Dunning, J. Chem. Phys. **90**, 1007 (1989).
[36] F. R. Bennett, A. D. J. Critchley, G. C. King, R. J. LeRoy, and I. R. McNab, Mol. Phys. **97**, 35 (1999).
[37] R. J. Le Roy, University of Waterloo Chemical Physics Research Report No. CP-329R3, 1993 (unpublished), available at http://leroy.uwaterloo.ca
[38] R. J. Le Roy, University of Waterloo Chemical Physics Research Report No. CP-555R, 1996 (unpublished), available at http://leroy.uwaterloo.ca